

**Initial susceptibility, flow curves, and magneto-optics of inverse magnetic fluids**

M. Raşa\* and A. P. Philipse

*Van 't Hoff Laboratory for Physical and Colloid Chemistry, Debye Institute, Utrecht University, Padualaan 8, 3584 CH Utrecht, The Netherlands*

D. Jamon

*Laboratory for Devices and Instrumentation in Optoelectronics and Microwaves, Jean Monnet University, 23, Rue dr. Paul Michelon, 42023 Saint-Etienne Cedex 2, France*

(Received 21 September 2002; revised manuscript received 15 April 2003; published 4 September 2003)

We introduce inverse magnetic fluids, consisting of gibbsite  $[\text{Al}(\text{OH})_3]$  platelets and alumina ( $\text{Al}_2\text{O}_3$ ) spheres dispersed in a magnetic fluid, studied together with silica ( $\text{SiO}_2$ ) dispersions based on the same magnetic fluid matrix. Atomic force microscopy, optical microscopy, and alternate gradient magnetometry confirm the remarkable stability of the samples. Optical microscopy shows aggregation of nonmagnetic spheres, which, surprisingly, strongly depends on the concentration of the magnetic fluid rather than the concentration of nonmagnetic particles. Our model for the initial susceptibility of inverse magnetic fluids agrees very well with experimental data for systems containing spherical particles. The flow curves in an external magnetic field are strongly influenced by the aggregation of nonmagnetic particles or preformed nonmagnetic particle clusters, and by their disruption due to the shear flow. Static linear magnetobirefringence and magnetodichroism of all samples are investigated both experimentally and theoretically. These effects, which occur in all magnetic fluids, can be enhanced by the additional anisotropy due to the magnetic holes. The experiments we performed showed that, at a wavelength of 820 nm, the magnetodichroism is increased while the magneto-birefringence decreases when nonmagnetic particles were dispersed in the magnetic fluid. Magneto-birefringence is expected to be increased at large enough wavelengths only.

DOI: 10.1103/PhysRevE.68.031402

PACS number(s): 82.70.-y, 75.50.Mm, 78.20.Ls, 83.80.Gv

**I. INTRODUCTION**

*Magnetic colloids* (called *magnetic fluids* or *ferrofluids*) [1,2], which consist of single domain magnetic particles (magnetite, iron or cobalt, for example) dispersed in organic polar or nonpolar solvents, have been prepared and studied for approximately 35 years. Even though the microstructure formation, particle interactions, and phase behavior of these systems are still debatable topics, many macroscopic properties together with their applications are known and widely used today [3].

In contrast to conventional magnetic fluids, much less is known about *inverse magnetic fluids*, composed of “non-magnetic” particles dispersed in a magnetic fluid. Although several studies on their magnetorheology have appeared (presented below), susceptibility results have been presented only by Volkova *et al.* [4], and only one hypothetical model of particle orientation for magnetobirefringence was published very recently by Pshenichnikov [5]. No measurements on magnetobirefringence and no results on magnetodichroism have been reported yet.

Highly monodisperse polystyrene spheres ( $1.9 \mu\text{m}$  in diameter) were for the first time dispersed in a kerosene-based magnetic fluid by Skjeltorp [6]. The nonmagnetic particles behave like magnetic holes, and, as a result of a strong attraction between them, rodlike chains parallel to the magnetic field were observed. At higher concentrations of magnetic holes “thick” chains formed [6]. Condensation and

ordering of such magnetic holes were studied by the same author in other papers [7–9], while dynamic susceptibility measurements were reported by Fannin *et al.* [10]. In Ref. [9] pear-shaped particles were dispersed and their structure imaged. Lu and Rosenblatt observed the orientation of large phospholipid thin hollow tubules ( $30 \mu\text{m}$  in length) in a magnetic fluid subjected to an external magnetic field [11]. Magnetorheological effect of inverse magnetic fluids containing spheres and large flaky particles ( $5\text{--}20 \mu\text{m}$  in size) was measured by Kashevskii *et al.* [12], while yield stress of dispersions of hollow glass beads ( $8 \mu\text{m}$  in diameter) in kerosene-based magnetic fluids (in the presence of a magnetic field) was measured by Popplewell and Rosensweig [13]. More detailed magnetorheological studies of practically monodispersed silica ( $400 \text{ nm}$  in diameter) spheres dispersed in a magnetic fluid matrix were done by de Gans *et al.* [14,15]. A comparison between inverse magnetic fluids and magnetorheological fluids, from the magnetorheological point of view, was done by Volkova in Ref. [4]. van Ewijk [16] observed and studied the attachment of magnetite particles from a magnetic fluid to the dispersed silica particles.

We dispersed different types of nonmagnetic particles in magnetic fluids based on nonpolar solvents (cyclohexane and decaline): silica spheres ( $\text{SiO}_2$ , approximately  $400 \text{ nm}$  in diameter), gibbsite platelets [ $\text{Al}(\text{OH})_3$ , approximately  $150 \text{ nm}$  in diameter and  $15 \text{ nm}$  in thickness], and alumina spheres ( $\text{Al}_2\text{O}_3$ , approximately  $400 \text{ nm}$  in diameter), all coated with suitable polymers. Gibbsite platelets and alumina spheres were dispersed in a magnetic fluid, in order to see the behavior of thin but highly anisotropic particles in the ferrofluid matrix, and to enhance the magneto-optical effects in inverse

\*Electronic address: m.rasa@chem.uu.nl

ferrofluids due to the higher refractive index of alumina, respectively. The properties of dispersed particles are presented in Sec. III A and the experimental techniques used for their characterization, as well as other techniques, are presented in Sec. II B.

These *nonmagnetic particles* (which have actually weak magnetic properties being either diamagnetic or paramagnetic) will be also referred to as *magnetic holes*. The behavior of nonmagnetic particles as magnetic holes is mainly related to their size, compared with the size of magnetic particles [14]: if the nonmagnetic particles are much larger than the magnetic particles, the magnetic fluid can be treated as a continuous medium and the nonmagnetic particles behave like magnetic holes in a continuous magnetizable medium. We anticipate that the alumina and silica spheres will behave like magnetic holes in the ferrofluid because of the much larger diameters in comparison with the diameters of magnetite particles, but it is questionable if this is true in the case of the very thin gibbsite platelets.

The “magnetic charges” induced at the interface of the two media allow one to assign a magnetic moment to such a hole. Different expressions for the apparent magnetic moment of a hole at low fields were proposed in Refs. [5,6,13,15]. For an isolated magnetic hole in an infinite continuous magnetic medium, the correct one is due to de Gans *et al.* [15]:

$$m = - \frac{\chi_{if}}{2} V H_a, \quad (1)$$

$$1 + \frac{1}{3} \chi_{if}$$

where  $\chi_{if}$  is the initial susceptibility of the ferrofluid,  $V$  is the volume of the spherical hole, and  $H_a$  is the applied field. This equation is in agreement with the results for a spherical hole in an infinite dielectric medium, rigorously derived in Ref. [17] and can be directly obtained if the electrical permittivity, polarization, and electric field strength are replaced by the magnetic permeability, magnetization, and magnetic field strength, respectively (this is allowed if there are no free currents and magnetization has no curl). The precise form of this equation is necessary for Eqs. (18) and (19). At higher fields, Eq. (1) must be generalized but for aggregated magnetic fluids it is no longer in agreement with the experimental observations, as it was observed in Sec. III D.

If the medium is finite, then the applied field must be corrected for the demagnetizing field, the corrected field being called internal field, which replaces  $H_a$  in Eq. (1). Since we correct the data for demagnetizing field (if any) in this paper, one can keep Eq. (1) formally unchanged but bear in mind that the magnetic field involved is the corrected field, throughout in this paper. Based on Eq. (1), the “magnetization” of the hole can be defined as  $M_h = m/V$  and its susceptibility as  $\chi_h = M_h/H_a$ . The orientation of the induced magnetic moment of the hole, opposite to the external field, and the high value of its susceptibility (of the order of ferrofluid susceptibility) resulted in the term of *apparent superdiamagnetism* for the particles immersed in a magnetic fluid. Thus, their intrinsic magnetic properties are irrelevant in this circumstance.

Magnetic properties of inverse magnetic fluids have been shown to be similar to those of the ferrofluids. In Ref. [18] a “dilution” formula was found experimentally from magnetometric measurements, i.e., the magnetization of the mixture is

$$M = M_f(1 - \Phi), \quad (2)$$

where  $M_f$  is the magnetization of the ferrofluid and  $\Phi$  is the volume fraction of the holes. However, at low fields, nonmagnetic particles are less aggregated into chains or even not aggregated and the field in the holes is different from the applied field. Thus we expect deviations from this result, and we investigated this aspect theoretically and experimentally for the case of silica inverse ferrofluids in Sec. III B.

Magnetorheological properties of the inverse magnetic fluids have been the most studied ones, in connection with their potential applications as magnetorheological fluids. In our study, we measured the flow curves for silica and gibbsite plates inverse ferrofluids, both in the presence and absence of a magnetic field, mainly to have additional information about aggregation or orientation of nonmagnetic particles. We report the first measurements of inverse magnetic fluids with the first commercially available magnetorheological cell (for Physica MCR 300 rheometer). The magnetorheological cell was developed for magnetorheological fluids, but we found that it can be employed for inverse ferrofluids too, though with some limitations for dilute inverse ferrofluids and magnetic fluids, as discussed in Sec. III C.

It is known that magnetic fluids exhibit strong static magnetobirefringence and significant magnetodichroism, as it was observed, for example, in Ref. [19]. We expect that by dispersing anisotropic nonmagnetic particles or if the spherical magnetic holes aggregate into chains, as it was already proved in Ref. [6], these effects will be enhanced. The measurements on all three types of inverse ferrofluids as well as theoretical models are presented in Sec. III D.

It is worth mentioning that the magnetic properties of inverse magnetic fluids (IMF) are determined by those of the magnetic fluid (MF) matrix [Eq. (2)], the magneto-optical properties of IMFs can be influenced by the magnetic holes in some extent, but the magnetorheological effect in the case of IMFs is practically determined by the structure formation of nonmagnetic particles, being much stronger than that of magnetic fluids, except for two cases: diluted IMFs and unstable magnetic fluids in which large elongated droplike aggregates can form. In the magnetorheological experiments the magnetic fluid serves mainly as the continuous fluid matrix which determines the moment  $m$  given by Eq. (1).

*Physical properties of magnetic fluids.* The magnetic properties of MF were studied experimentally, among others, by Raşa *et al.* [20]. Several models for particle interactions and aggregate formation taken from literature are also presented and discussed in the same paper. Physically, the magnetic moments of single domain particles, randomly oriented due to the Brownian motion, tend to align to the external field, but this *orientation process* is influenced by particle interactions. One of the models for interacting particles,

which gave good results in several cases, is the thermodynamic perturbation theory (TPT) [21,22]. Besides the equation for magnetization it yields the effective field inside the ferrofluid:

$$H_{\text{eff}} = H_a + \frac{1}{3}M_L + \frac{1}{144}M_L \frac{dM_L}{dH_a}, \quad (3)$$

where  $M_L$  is the ideal (Langevin) magnetization of the system (as if there were no particle interactions). Aggregation occurs if the dipole-dipole interaction energy of particles is larger than the thermal energy; it strongly depends on the ferrofluid type, resulting in a large variety of clusters from short chains of a few particles to very large agglomerations of millions of particles. Thus, the few existing models have only a very limited area of validity.

The magnetorheological effect in a stable MF is determined by the same orientational and agglomeration processes, but an additional observation is necessary: only Brownian particles (which rotate together with their magnetic moment relative to the solvent) contribute to the orientation mechanism. For low concentrations (negligible interactions and aggregates), the Shliomis model predicts [23]

$$\eta_f(H_a) = \eta_f(0) \left( 1 + \frac{3}{2} \Phi_{0h} \frac{\xi - \tanh \xi}{\xi + \tanh \xi} \sin^2 \beta \right), \quad (4)$$

where  $\eta_f(0)$  is the viscosity of the magnetic fluid in zero field,  $\Phi_{0h}$  is the hydrodynamic volume fraction of the magnetic particles,  $\beta$  is the angle between the external field  $H_a$  and vorticity, and  $\xi = \mu_0 m_m H_a / (kT)$  is the Langevin parameter.  $\mu_0$  is the magnetic permeability of vacuum,  $m_m$  is the magnetic moment of a magnetic particle,  $k$  is Boltzmann's constant and  $T$  is the absolute temperature. This model can be improved [24] by taking into account the lognormal size distribution of particles:

$$f(x) = \frac{1}{xS\sqrt{2\pi}} \exp \left( -\frac{\ln^2 \frac{x}{D_0}}{2S^2} \right), \quad (5)$$

where  $x$  is the diameter of particles,  $D_0$  is defined by  $\ln D_0 = \langle \ln x \rangle$ , and  $S$  is defined as the mean deviation of  $\ln x$  from its mean value.

Magneto-optical properties of MF are determined by the same processes of Brownian orientation and agglomeration of magnetic particles, but in this case the important aspect is the deviation from the spherical shape of particles or of their clusters. Models of particle orientation and chaining and experimental data are presented, for example, in Refs. [19,25]. For the case of diluted samples, an orientation model due to Raša [26] gives the dielectric tensor of a magnetized ferrofluid. The diagonal components are

$$\varepsilon_{11} = \varepsilon_{22} = \frac{(1 - \Phi_0)\varepsilon_1 + \Phi_0 \left( \varepsilon'_\perp + (\varepsilon'_\parallel - \varepsilon'_\perp) \frac{L(\xi)}{\xi} \right)}{(1 - \Phi_0) + \frac{\Phi_0}{\varepsilon_2} \left( \varepsilon'_\perp + (\varepsilon'_\parallel - \varepsilon'_\perp) \frac{L(\xi)}{\xi} \right)}, \quad (6)$$

$$\varepsilon_{33} = \frac{(1 - \Phi_0)\varepsilon_1 + \Phi_0 \left( \varepsilon'_\parallel + 2(\varepsilon'_\perp - \varepsilon'_\parallel) \frac{L(\xi)}{\xi} \right)}{(1 - \Phi_0) + \frac{\Phi_0}{\varepsilon_2} \left( \varepsilon'_\parallel + 2(\varepsilon'_\perp - \varepsilon'_\parallel) \frac{L(\xi)}{\xi} \right)}, \quad (7)$$

in which  $\varepsilon_1$  is the real scalar permittivity of solvent,  $\varepsilon_2$  is the complex permittivity of magnetite,  $\Phi_0$  is the volume fraction of magnetic particles,  $L(\xi) = \coth \xi - 1/\xi$  is the Langevin function,  $\varepsilon'_\perp = \varepsilon_1 \varepsilon_2 / [\varepsilon_1 + (\varepsilon_2 - \varepsilon_1)n_\perp]$  and  $\varepsilon'_\parallel = \varepsilon_1 \varepsilon_2 / [\varepsilon_1 + (\varepsilon_2 - \varepsilon_1)n_\parallel]$ .  $n_{\perp,\parallel}$  are the depolarization coefficients perpendicular and parallel to the anisotropy axes of spheroidal identical particles, respectively. For more concentrated samples, replacing of the external field with an effective field was proved to give very good results [27]. Following Ref. [26], the birefringence (actually the phase lag between the ordinary and extraordinary waves) is given by

$$\theta = \frac{2\pi l}{\lambda_0} [\sqrt{\text{Re}(\varepsilon_{33})} - \sqrt{\text{Re}(\varepsilon_{11})}], \quad (8)$$

where  $l$  is the thickness of the sample and  $\lambda_0$  is the wavelength in vacuum. In the dilute limit, the birefringence is proportional to [27]

$$\theta \propto \frac{\pi l \Phi_0 \left( 1 - \frac{3L(\xi)}{\xi} \right)}{\lambda_0}, \quad (9)$$

exactly the same relation being valid for dichroism [28], which is defined as the difference between the imaginary parts of the refractive indices of extraordinary and ordinary waves, respectively.

## II. EXPERIMENTAL DETAILS

### A. Samples

The *magnetic fluid*, prepared by D. Bica [29], contains magnetite particles, covered with purified oleic acid and dispersed in cyclohexane.

Powders of *silica* particles, coated with stearyl alcohol as described in Ref. [30], were redispersed in cyclohexane.

*Gibbsite* [ $\text{Al}(\text{OH})_3$ ] platelets, dispersed initially in water according to Ref. [31], were covered with modified polyisobutene (PIB) provided by Shell (code SAP 230), and redispersed in cyclohexane, following the method described in Ref. [31].

Commercial  $\alpha$ -*alumina* powder (Sumitomo) was first dispersed in demi-water under stirring and sonication and left for hydration 24 h. Then, the same method [31] used for gibbsite platelets was employed to irreversibly graft the surface of the particles with PIB and to redisperse them in cyclohexane. Gravitational sedimentation was used to remove aggregates while centrifugation was used to remove the excess of polymer by repeatedly replacing the supernatant with pure solvent.

The *inverse magnetic fluids* were prepared in two ways: (1) the magnetic fluid was simply mixed with the nonmagnetic dispersion benefitting from the use of the same solvent

and the same type of stabilization (the steric one) in all samples and (2) the nonmagnetic particles were dried and then redispersed in the magnetic fluid as described in the following subsection (item susceptibility measurements).

### B. Experimental techniques and details

*Atomic force microscopy (AFM).* A multimode AFM (Nanoscope IIIa, Digital Instruments) was used to image the magnetic and nonmagnetic colloidal particles. Particles from very diluted dispersions were spread on a freshly cleaved mica substrate, which was spun until the sample dried. The obtained specimen was scanned with standard silicon tips (TESP, Digital Instruments) in tapping mode [32].

*Optical microscopy.* A Zeiss Axiolab microscope with an 100 $\times$  objective was used to image *in situ* structures of particles in the ferrofluid and inverse ferrofluids. VitroCom (glass) flat capillaries, with an optical path of 0.05 mm, were used as optical cells. The maximum uniform magnetic field was  $B=0.1$  T. The images were acquired with a CCD camera.

*Susceptibility measurements* were done with a KLY-3S Kappabridge susceptometer (AGICO). The applied field is 300 A/m at a frequency of 875 Hz. The volume fraction dependence of susceptibility of silica inverse ferrofluids was measured. Silica particles (in different amounts) were dried and redispersed in the magnetic fluid. The system was alternately stirred (a couple of hours) and sonicated (5–20 min) until a homogeneous mixture was obtained. The volume fraction of silica in each sample was determined from density and mass measurements. The susceptibility was measured at constant temperature ( $22 \pm 0.2$  °C) using a thin cylinder completely filled and sealed, oriented parallel to the field. The measured accuracy was 0.05% and the measured reproducibility was 0.3%. Data were corrected for the small demagnetizing field.

*Magnetization measurements* were performed with an Alternating Gradient Magnetometer (AGM) (Micromag 2900, Princeton Measurements). The sample holder was a very thin flat capillary glass, placed with the narrow section perpendicular to the magnetic field. In this case, the demagnetizing field is completely negligible.

*Static light scattering (SLS)* was used for size determination of nonmagnetic particles. Very dilute dust free samples were measured for this purpose by using a FICA 50 setup. The wavelength of the incident linearly polarized light was  $\lambda_0=436$  nm.

*Dynamic light scattering (DLS)* was performed with a home made setup using a Malvern 7032 CE correlator (128 channels) on the same samples designed for SLS. The wavelength of the incident linearly polarized light was 647.1 nm.

*Rheological and magnetorheological measurements* were done with a Physica MCR 300 rheometer (Anton Paar). In zero magnetic field, the cone-plate CP-50 1 geometry was preferred because we could perform measurements at lower shear rates. The commercial magnetorheological cell PP 20/MR, which is a plate-plate measuring system, was used to obtain flow curves at different values of the applied field. The distance between the plates was adjusted to optimize the

sensitivity and varied between 0.2 and 0.4 mm. Magnetite particles were transferred to decaline to prevent evaporation during depositing the layer of the magnetic fluid on the inferior plate. The inverse ferrofluids were prepared as for susceptibility measurements but using decaline-based magnetic fluids. The maximum field in vacuum between the two plates is 0.43 T. The reproducibility was dependent on the shear rate values. In most cases the measurements were not reproducible at low shear rates (due to the irreversible microstructural changes determined by the shear flow) but the reproducibility was good at higher shear rates (above  $50 \text{ s}^{-1}$ ). Consequently, the sample, which was left in the external field enough time (approximately 10 min) before measuring the magnetoviscous effect, was replaced before a new measurement was performed.

*Linear static magnetobirefringence and dichroism* measurements were done with a null ellipsometry setup, described, together with the determination of birefringence and dichroism, in Refs. [33,34]. The laser beam passes through a thin layer of fluid and the polarizers are rotated until the amplitude of the first harmonic of the modulated light intensity vanishes. The birefringence and dichroism are determined from the rotation angles of the polarizers. The dispersions were prepared as for susceptibility measurements. The solvents were cyclohexane and decaline. For cyclohexane based samples we used flat capillary glass (VitroCom) completely filled and sealed with glue, while for decaline-based samples we used detachable glass plates. The optical path was in both cases 0.1 mm and the wavelength  $\lambda_0=820$  nm. In the case of birefringence the accuracy is 1°, while the reproducibility is about 2.5% in the case of using capillaries.

*Other techniques.* Densities were accurately measured with a DMA 5000 Anton Paar densimeter and sedimentation was performed with a L-60 Beckman ultracentrifuge.

## III. RESULTS AND DISCUSSIONS

### A. Characterization of particles and dispersions

*Magnetic fluid.* Particle analysis in magnetic fluids was done by using magnetization curves and AFM pictures. The magnetization curve of a very dilute sample allows the determination of the mean magnetic diameter of magnetite particles  $\langle D_m \rangle$  and standard deviation  $\sigma$ , according to Eqs. (13) and (14) derived and presented in Ref. [24]. The physical diameter  $\langle D \rangle$  is obtained after adding the thickness of the nonmagnetic layer of the particles, which for magnetite nanoparticles is 1.7 nm [2]. The AFM pictures allow to determine the mean lateral diameter and mean height of particles  $\langle h_{AFM} \rangle$ . Since the first is strongly overestimated due to the tip convolution [32], only the latter can be reliable. However, we observed that the underestimation of  $\langle h_{AFM} \rangle$ , is not only due to the small deviation from the spherical shape of the particles [32], but also because of the tip-substrate interaction, being also influenced by the scanning parameters (like amplitude setpoint and drive frequency). This explains the difference in the values obtained and presented in Table I.

TABLE I. Magnetite, silica, and gibbsite particle analysis.

Particle	$\langle D_m \rangle$ (nm)	$\sigma$ (nm)	$\langle D_{SLS} \rangle$ (nm)	$\sigma_{SLS}$ (nm)	$D_{SLS}$ (nm)	$D_{DLS}$ (nm)	$\langle h_{AFM} \rangle$ (nm)	$\langle D_{AFM} \rangle$ (nm)
Magnetite	7.8	2.33					6.8	
Silica					380	391	330	
Gibbsite			131	25			13.8	152

The stock magnetic fluid we used here exhibits aggregates observed even with the optical microscope. Previous investigations on similar magnetic fluids, but based on nonevaporating solvents [20], showed very short chains (mostly dimers and trimers) and important particle interactions above volume fractions of 1%. The presence of aggregates in the stock sample we used in this paper might be a result of cluster formation on the bottle walls due to the fast-evaporating cyclohexane solvent (the sample was prepared two years ago). These clusters behave like centers of nucleation for reversible thick chain formation in external field, as observed by optical microscopy.

*Silica particles.* The mean diameter of silica particles was determined from SLS measurements from the first minimum ( $D_{SLS}$ ) of the scattered intensity profile. The fit of the scattered intensity, done by using the form factor for spherical particles [35] and lognormal size distribution [Eq. (5)], failed, indicating the presence of some aggregates (the presence of impurities is not excluded too). The mean height of particles was determined from AFM pictures and the hydrodynamic diameter  $D_{DLS}$  from DLS measurements. They are in fairly good agreement: the hydrodynamic diameter is always larger than the SLS diameter while both of them are larger in this case than the AFM height mainly because of the presence of aggregates. The results are also presented in Table I. The second cumulant analysis [36], tried on DLS data, failed, indicating a polydispersity significantly larger than 5%. This confirms the aggregate presence.

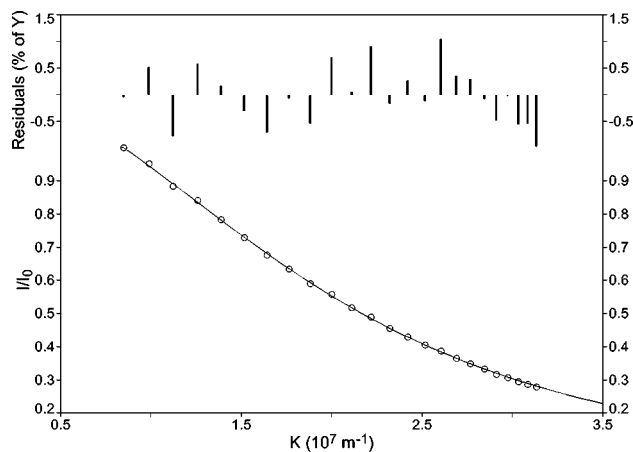


FIG. 1. Fitted relative scattered intensity vs  $K = (4\pi/\lambda_0)\sin(\theta/2)$ , where  $\theta$  is the scattering angle. The measured intensities are normalized by  $I_0$ , which is the scattered intensity at the smallest measured angle ( $30^\circ$ ). Fit residual bars are plotted above.

*Gibbsite plates.* The mean diameter of gibbsite plates ( $\langle D_{SLS} \rangle$ ) and standard deviation  $\sigma_{SLS}$  were determined from SLS after a good fit (Fig. 1), by using the form factor for very thin disks [37] and the lognormal size distribution. The mean diameter was also determined from AFM measurements,  $\langle D_{AFM} \rangle$  (tip convolution in this case is negligible [32]), together with the mean height  $\langle h_{AFM} \rangle$  (Table I).

*Commercial  $\alpha$ -alumina particles* have a mean physical diameter of 400 nm but the AFM and TEM pictures show a higher polydispersity in size and shape than in the case of silica particles.

*Inverse magnetic fluids.* The mixtures of the magnetic fluid with nonmagnetic colloids showed a remarkable stability. Eye inspection was completed with optical microscopy observation, AFM pictures of diluted mixtures, and magne-

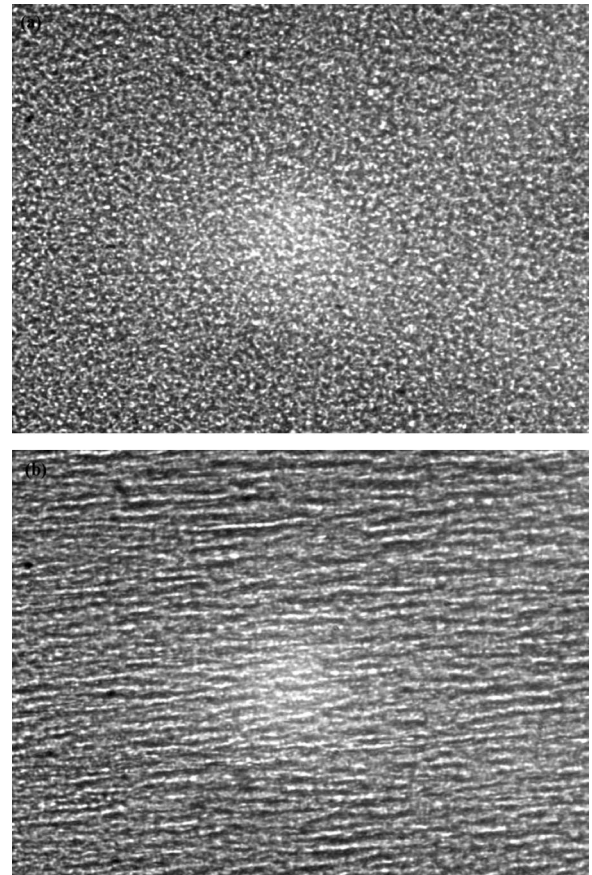


FIG. 2. Optical microscopy image ( $100 \times 75 \mu\text{m}$ ) of alumina inverse magnetic fluid in zero field (a) and in a 0.1 T external field (b). The ferrofluid contains 10% vol magnetite particles.

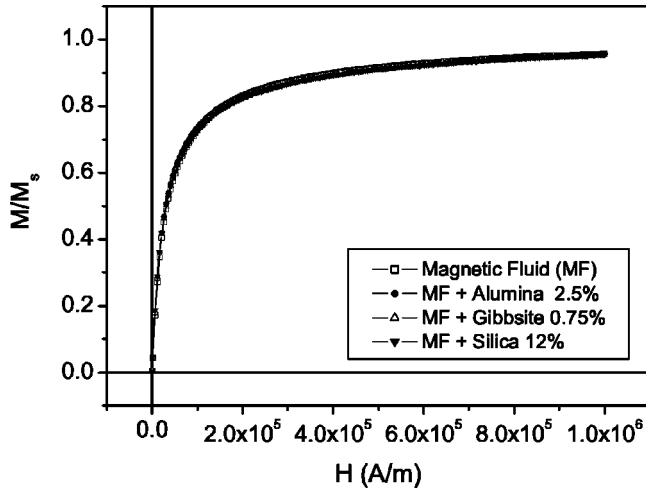


FIG. 3. Reduced magnetization curves for inverse and pure magnetic fluids.

tization measurements, done for the samples that were measured in Sec. III C.

Optical microscopy showed homogeneous dispersions in all cases. In the case of ferrofluids and platelets inverse ferrofluids, visible features appeared only in the presence of a magnetic field, because of aggregation of magnetic particles. No visible aggregates of plates could be observed. In the case of silica and alumina inverse ferrofluids, the images were similar. The image in zero field is different from the ferrofluid image and the applied field induces larger aggregates than those observed in the ferrofluid due to magnetic hole chaining (Fig. 2).

Magnetization curves (Fig. 3) measured with AGM showed no microstructural changes in the magnetic phase

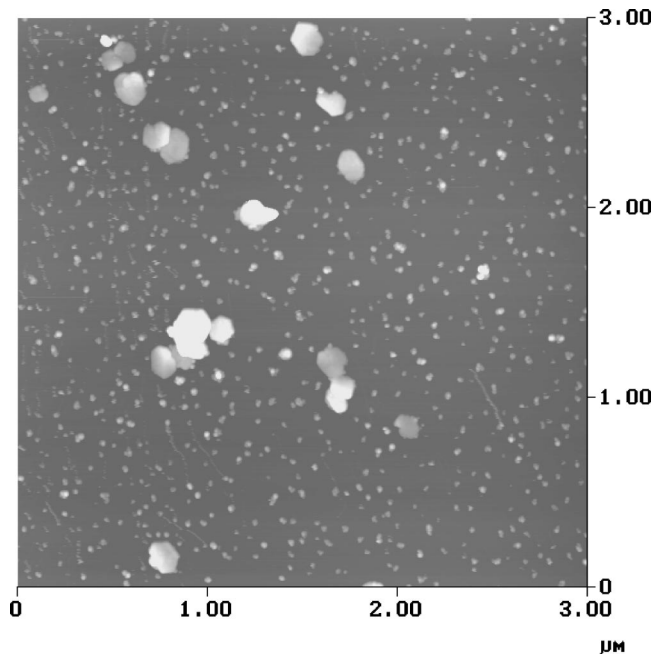


FIG. 4. AFM height image of gibbsite platelets dispersed in a magnetic fluid. The smaller features are the magnetite particles.

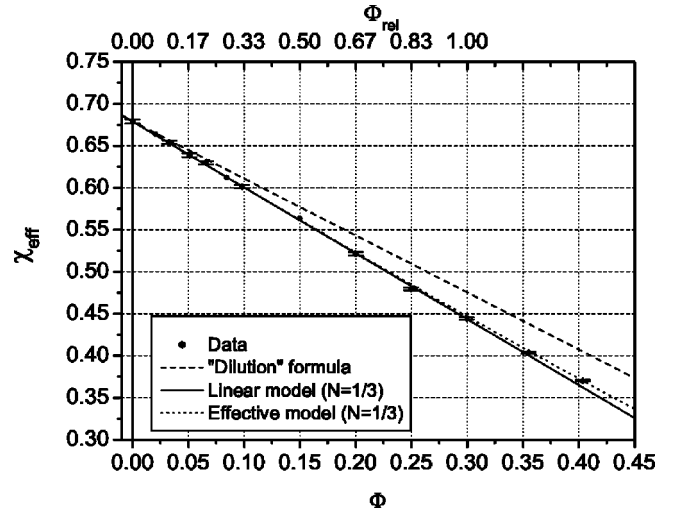


FIG. 5. Susceptibility of silica inverse magnetic fluids vs volume fraction  $\Phi$  of silica. The top scale is relative to the volume fraction  $\Phi = 0.3$  considered unity. Equations (16) and (20) are referred to as the linear and effective models, respectively.

after dispersing nonmagnetic particles: reduced magnetization curves stay superimposed.

AFM pictures (an example for the plates inverse ferrofluid is given in Fig. 4) show a high degree of dispersion of nonmagnetic particles among magnetite colloids. However, it was difficult to obtain good AFM images because of aggregation of particles on the mica substrate due to capillary forces, which act on the particles during drying of the thin layer of colloid, and result mainly in two-dimensional cluster formation.

### B. Initial susceptibility of silica inverse magnetic fluids

The initial susceptibility of silica inverse ferrofluids versus volume fraction of silica, measured as described in Sec. II B, is presented in Fig. 5. The “dilution” formula [Eq. (2)], now written for susceptibilities, is not in good agreement with the data, and this is because the field in the silica particles, not aggregated at such a small external field, is different from the applied field. In order to calculate the susceptibility of silica IMF we considered the magnetic fluid a continuous medium with the initial susceptibility  $\chi_{if}$ , in which silica spheres are dispersed. The definition of the effective permittivity of a mixture given in Ref. [38] is rewritten here for magnetostatics as

$$\langle B \rangle = \mu_{\text{eff}} \langle H \rangle, \quad (10)$$

where, for example,

$$\langle H \rangle = \frac{1}{V_t} \left( \int_{V_f} H_1 dV + \int_{V_{NM}} H_2 dV \right) \quad (11)$$

is the field strength averaged over volumes  $V_t$  much larger than the volume of a silica particle (the same for the  $B$  field). Index 1 corresponds to the magnetic fluid matrix of volume  $V_f$  and index 2 corresponds to silica particles of total volume  $V_{NM}$ , so that  $V_t = V_f + V_{NM}$ . For spheres and in the more

general case of ellipsoids, the field inside particles is uniform. The demagnetizing factor of a magnetic hole in the direction of the field is denoted by  $N$ . If the volume fraction  $\Phi$  of nonmagnetic particles is very low, then the mean fields can be easily written as follows:

$$\langle H \rangle = (1 - \Phi)H_1 + \Phi H_2, \quad (12)$$

$$\langle B \rangle = (1 - \Phi)B_1 + \Phi B_2. \quad (13)$$

At very low  $\Phi$ , the field in the ferrofluid is  $H_1 = H_a$ . Then,  $B_1 = H_a + M_1$  where  $M_1 = \chi_{if}H_a$  is the magnetization of the ferrofluid at low fields. The field  $H_2$  inside a magnetic hole is given by

$$H_2 = \frac{1 + \chi_{if}}{1 + \chi_{if} - N\chi_{if}} H_a \quad (14)$$

and can be easily obtained from the expression of the electric field inside a dielectric ellipsoid in an external field [39], replacing the electrical permittivity by  $1/\mu$ , where  $\mu$  is the magnetic permeability ( $\mu = 1 + \chi$ ). This is because of the fact that in our case we deal with a hole in a polarized medium and the replaced permittivity must be inverted [17]. Taking into account that in a hole  $B_2 = H_2$ , one obtains

$$\chi_{\text{eff}} = \chi_{if} - \frac{\Phi(1 + \chi_{if})\chi_{if}}{1 + \chi_{if} - \chi_{if}(1 - \Phi)N}. \quad (15)$$

It is correct to linearize this equation since it is valid at low  $\Phi$  only. One obtains

$$\chi_{\text{eff}} = \chi_{if} \left[ 1 - \frac{(1 + \chi_{if})}{1 + \chi_{if}(1 - N)} \Phi \right] \quad (16)$$

in agreement with Ref. [38]. We can see that a ‘‘dilution’’ formula [ $\chi_{\text{eff}} = \chi_{if}(1 - \Phi)$ ] is obtained only for long rods, if the external field is strong enough for keeping them aligned; then  $N \rightarrow 0$ . In our case  $N$  should be close to  $1/3$  because of the practically monodisperse (in shape) silica spheres. At 300 A/m, the dipole-dipole energy between two silica spheres is much smaller than the thermal energy (their ratio is 0.005), so we do not expect aggregates (induced by the field) which would modify the value of  $N$ . The possible anisotropic aggregates present in the system may influence the value of  $N$  only if their volume is large enough to be aligned by the weak magnetic field.

We can see from Fig. 5 that the data points are in very good agreement with Eq. (16) at low and even medium volume fractions, while at high volume fractions there is a small deviation. This is because of the field produced by the silica particles. The top scale in this figure was obtained after making some successive dilutions from the sample with  $\Phi = 0.3$ , considered with a relative volume fraction equal to unity. It was used to fit the low fraction data points with Eq. (16) and to determine the volume fraction of the silica spheres in the original silica dispersion. Assuming  $N = 1/3$ , we obtained  $\Phi_s = 12.26\%$ , which is very close to the value 12.30%, determined from density and mass measurements.

At higher volume fractions of holes, we may replace the applied field  $H_a$  that acts on the magnetic particles in the ferrofluid with an effective field  $H_{\text{eff}}$  determined by the polarized silica spheres. It can be perturbatively introduced, as it was done for pure ferrofluids by Ivanov [22] [Eq. (3)], because of the very weak dipole-dipole interaction energy of magnetic holes in comparison with the thermal energy. In the first order,

$$H_{\text{eff}} = H_a + \frac{1}{3}M_{NM}, \quad (17)$$

but now  $M_{NM}$  is the magnetization of the magnetic hole subsystem. The factor  $1/3$  changes if magnetic holes with various shapes would be dispersed or if the spheres are aggregated. Because their magnetic moments are always parallel (but oppositely oriented) to the external magnetic field, we have

$$M_{NM} = \Phi M_h, \quad (18)$$

where  $M_h$  is the (virtual) magnetization of one particle, i.e.,  $M_h = m/V$ , with  $m$  given by

$$m = - \frac{\chi_{if}}{1 + \chi_{if}(1 - N)} V H_a, \quad (19)$$

which is a generalization of Eq. (1) for ellipsoids. Following the same procedure as for low  $\Phi$ , we obtain for the effective initial susceptibility,

$$\chi_{\text{eff}} = \chi_{if} - \frac{\Phi(1 + \chi_{if})\chi_{if}}{1 + \chi_{if} - \chi_{if}(1 - \Phi)N - \frac{1}{3}(1 - \Phi)\Phi\chi_{if}}. \quad (20)$$

A very good agreement with data can be seen in Fig. 5.

At higher fields aggregates form. They will reduce the value of  $N$  down to 0. At quas saturation, the applied field is also much higher than that produced by the holes, so that the magnetization of the inverse ferrofluid is simply reduced by the factor  $1 - \Phi$ , as it was found in Ref. [14]. This fact is useful for estimating the volume fraction of nonmagnetic particles from the saturation magnetization.

### C. Flow curves of inverse magnetic fluids

*The flow curves in zero field* of the magnetic fluid (the volume fraction of magnetite was  $\Phi_0 = 10\%$ ), silica inverse magnetic fluids ( $\Phi = 2.5\%$  and  $10\%$ ), and plates inverse magnetic fluids ( $\Phi = 2.5\%$ ) are presented in Fig. 6. The same magnetic fluid was used as a solvent matrix for all the composites studied in this paragraph. The magnetic fluid showed a Newtonian behavior in the range of shear rates  $\dot{\gamma} \in (2, 10^3) \text{ s}^{-1}$ , at which we had enough sensitivity to measure. This behavior is consistent with the assumption that in zero field the clusters are small. The silica 2.5% inverse magnetic fluid is non-Newtonian at low shear rates, but for  $\dot{\gamma}$  between 200 and  $10^3 \text{ s}^{-1}$  is also Newtonian. The translational Peclet number

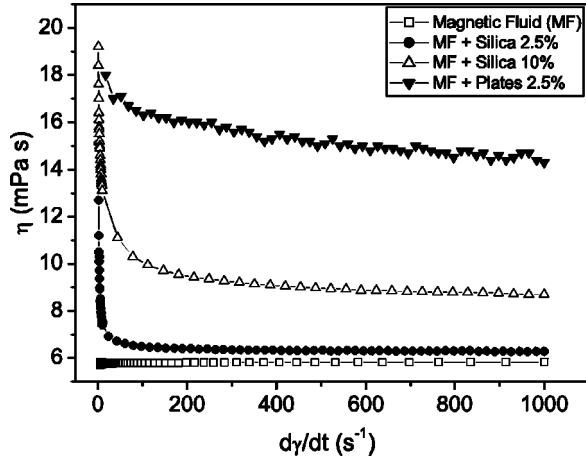


FIG. 6. Apparent viscosities in the absence of external magnetic field vs shear rate.

$$Pe^t = \frac{\eta_0 R^3 \dot{\gamma}}{kT}, \quad (21)$$

where  $\eta_0$  is the viscosity of the carrier liquid (the magnetic fluid in our case) and  $R$  is the radius of the spheres, is slightly larger than 1 only if  $\dot{\gamma} > 120 \text{ s}^{-1}$ . At these values, however, the shear thinning is negligible. Since the concentration of silica is relatively low for particle interactions, we consider that the shear thinning behavior at low shear rates is mainly determined by the silica clusters that are disrupted by the shear flow, decreasing the viscosity towards its Newtonian limit. The presence of some silica aggregates (due to van der Waals interactions) in zero field is in agreement with the observations based on the SLS and DLS measurements. In addition, redispersion of dried particles may leave more aggregates behind while the sample concentration is higher than in the case of light scattering measurements. The viscosities ( $\eta$ ) determined by linear fit (for 2.5% silica IMF from the linear part only) are found in Table II.

The 10% silica IMF is non-Newtonian in the whole range measured, suggesting a higher concentration of aggregates and significant interactions between silica particles in this more concentrated system. The 2.5% plates IMF is also non-Newtonian, showing larger apparent viscosities than the 2.5% silica IMF. In zero field, unlike the previous samples, it was measured with the magnetorheological cell, thus we could not go to lower shear rates. In addition to aggregates

breaking, flow-induced orientation may now further decrease the viscosity if the rotational Peclet number for single platelets,

$$Pe^r = \frac{32 \eta_0 R^3 \dot{\gamma}}{3kT}, \quad (22)$$

is significantly larger than 1. Here  $R$  is the radius of the disk. For  $\dot{\gamma} > 175 \text{ s}^{-1}$  the Peclet number is larger than 1, so that the orientation of particles contributes to the decrease of viscosity at high shear rates only, while the aggregate disruption at low rates. However, because of the larger viscosities in comparison to 2.5% silica IMF at high shear rates, flow-induced orientation does not seem to play an important role.

The simplest and frequently used law for describing non-Newtonian fluids is the power law:

$$\tau = m \dot{\gamma}^n, \quad (23)$$

where  $\tau$  is the shear stress and  $m$  and  $n$  are fit parameters. The fit to the data for the non-Newtonian systems is good for medium shear rates (more details in the following paragraph) but it was not satisfactory at low rates. In addition, the inverse ferrofluids measured in this paper become or tend to become Newtonian, thus a better agreement with the data was found if we consider the following function:

$$\tau = m \dot{\gamma}^n + \eta_\infty \dot{\gamma}, \quad (24)$$

which describes explicitly the asymptotic Newtonian regime and yields its viscosity  $\eta_\infty$ . A better description in the low rate range was obtained. The disadvantage is the larger number of fit parameters; nevertheless, the value of  $\eta_\infty$  for 2.5% silica IMF is very close to that obtained from the Newtonian part of the flow curve (Table II). A good fit to the apparent viscosity (defined as  $\tau/\dot{\gamma}$ ) of 10% silica IMF with the apparent viscosity given by Eq. (24) is shown in Fig. 7.

The flow curves in a magnetic field were measured with the magnetorheological cell. Built for magnetorheological fluids [40], it also appears useful for measuring magnetic fluids and their composites. The only drawback is the lack of sensitivity at low shear rates for magnetic fluids and dilute inverse magnetic fluids (we could not measure them below  $80\text{--}100 \text{ s}^{-1}$ ). On the contrary, in the case of 10% silica IMF we could measure in the whole possible range of shear rates, i.e.,  $\dot{\gamma} \in (10^{-2}, 10^3) \text{ s}^{-1}$ .

TABLE II. Viscosity  $\eta$  of the Newtonian sample or determined from the Newtonian region at high shear rates and the viscosity at high shear rates  $\eta_\infty$  of inverse magnetic fluids, in the absence and presence of a magnetic field  $H$ .

Sample	$\eta (H=0)$ (mPa s)	$\eta_\infty (H=0)$ (mPa s)	$\eta (H=313 \text{ kA/m})$ (mPa s)	$\eta_\infty (H=63.7 \text{ kA/m})$ (mPa s)
1. Magnetic fluid	$5.83 \pm 1.0 \times 10^{-3}$		$8.17 \pm 2.0 \times 10^{-2}$	
2. MF+silica 2.5%	$6.25 \pm 6.9 \times 10^{-3}$	$6.23 \pm 9.0 \times 10^{-3}$		$7.16 \pm 8.5 \times 10^{-2}$
3. MF+silica 10%		$7.80 \pm 4.9 \times 10^{-2}$		$8.78 \pm 0.26$

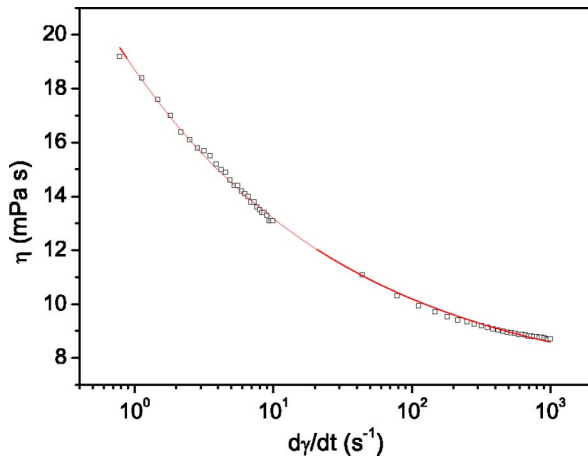


FIG. 7. Fit with the apparent viscosity given by Eq. (24) to the measured apparent viscosity of 10% silica inverse ferrofluid, as a function of shear rate.

The magnetic fluid exhibited a magnetorheological effect of 40% according to Fig. 8, where the viscosity at the maximum field (313 kA/m) was plotted together with the viscosity in zero field. In the measured range it remained Newtonian. The Shliomis model [Eq. (4)] cannot be applied to estimate the particle orientation contribution to the magnetoviscous effect because of the large aggregate formation in the presence of the field. We observed however that, in the shear rate range in which we could measure, it gives a good estimation of the order of magnitude of the effect, probably because the aggregates are significantly reduced in size by the shear flow. But the study of how this model works is not our goal in this paper.

The magnetic flux density in the sample can be calculated by using the following equation [40]:

$$B = 7.539 \times 10^{-4} \frac{I}{0.0035 - d(1 - 1/\mu_r)} \text{ [T]}, \quad (25)$$

where  $I$  is the current intensity (in A) through the coil which produces the magnetic field,  $d$  is the gap between the cell

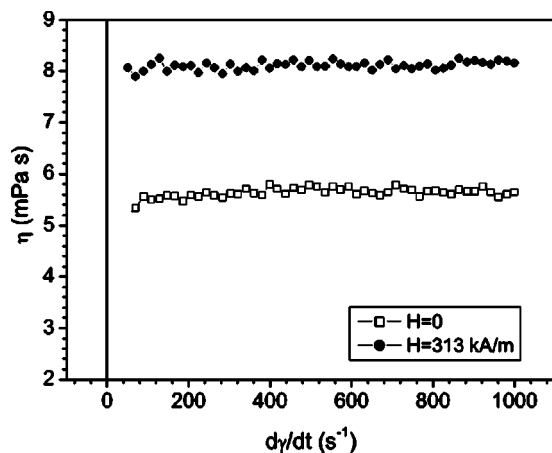


FIG. 8. Viscosity of the pure magnetic fluid with a volume fraction of magnetite of 10% in the absence and in the presence of an external magnetic field vs shear rate.

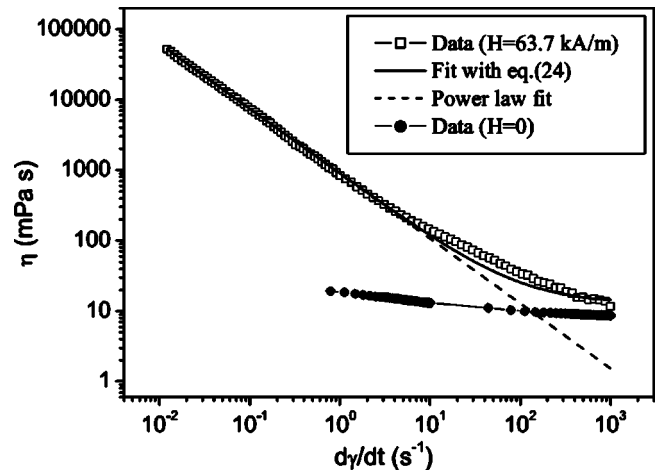


FIG. 9. Fitted apparent viscosity of the 10% silica inverse magnetic fluid in the presence of a field of 63.7 kA/m, vs shear rate. Apparent viscosity in zero field is shown for comparison.

plates (in m), and  $\mu_r = 1 + \chi$  is the relative magnetic permeability of the sample. The field strength is given by  $H = B/(\mu_0\mu_r)$ . The relative permeability is constant at very low fields only. At high fields it tends to 1. Since our samples have an initial susceptibility close to 1, we will make an error below 6% (decreasing to zero with the field) if we use the relative permeability of vacuum in Eq. (25). The demagnetizing field was not taken into account in Eq. (25), so that  $H_d = -NM$  must be subtracted from the applied field. The demagnetizing factor  $N$  is practically 1 and  $M$  (the magnetization of the sample) is obtained from the interpolation of the magnetization curve for the applied field value in air. This final value is mentioned in this paper.

The viscosity of silica IMFs is strongly affected by the magnetic field. As an example, the flow curve for 10% silica IMF at 63.7 kA/m is shown in Fig. 9. The chains formed by the magnetic holes (due to dipole-dipole interactions) significantly modify the viscosity of the sample, which exhibits a shear thinning effect due to chain disruption. The effect was observed for 2.5% silica IMF too, but it was measured with much lower accuracy in the low rate region, because of the smaller viscosities achieved. The fit to the data of Fig. 9 with Eq. (24) was better than with the power law. However, Eq. (24) does not describe accurately the flow curve over the entire range of  $\dot{\gamma}$ .

The 2.5% plates IMF, in the presence of the external field, has lower viscosities in the low rate region in comparison to 2.5% silica IMF, which made the measurements below  $50 \text{ s}^{-1}$  impossible (Fig. 10). At high shear rates the apparent viscosity was larger. In addition to the contribution of the magnetic fluid matrix to the effect, aggregate formation, smaller than in the case of silica IMFs (not observed optically) but more anisometric, can explain the experimental facts. At high fields, not only the magnetoviscous effect was larger than that of the pure magnetic fluid but also the non-Newtonian behavior was more pronounced. The orientation of plates by the magnetic field (parallel to the field), if it occurs, may also increase the viscosity while the flow-induced orientation (which tends to align plates perpendicu-

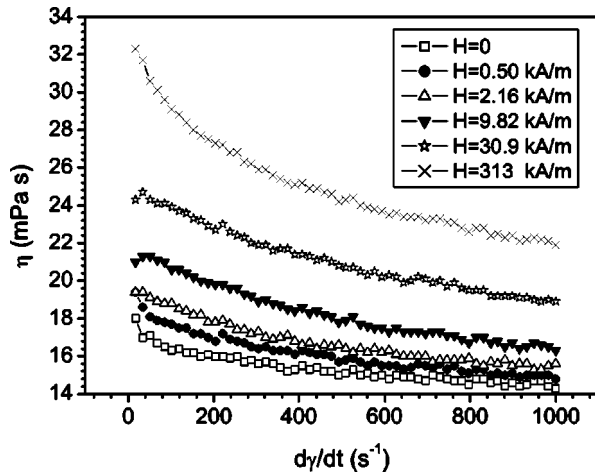


FIG. 10. Apparent viscosity of the 2.5% plates inverse magnetic fluid for different external magnetic fields vs shear rate.

lar to the external field) can contribute to the shear thinning at high rates only. Taking into account the behavior in zero field, where shear thinning was mainly due to aggregate disruption, we consider that this is the dominant effect in the presence of magnetic fields too. More concisely, the preformed clusters (observed in zero field) serve as nuclei for chaining, behaving as magnetic holes; we may not conclude that the same thing is valid for single plates neither from the data nor phenomenologically, because of their too small volume and thickness. That is why the field orientation of particles is also considered not significant. For plates IMF, the power law describes well the data for this narrow range of  $\dot{\gamma}$ , too narrow for a three-parameter fit with Eq. (24), which was unsuccessful. To show the validity of the power law in this region, we calculated numerically the ratio  $\tau/\eta$ , which should vary linearly with  $\dot{\gamma}$  if Eq. (23) is valid. The measured shear stress was smoothed and divided by the numerically calculated derivative of the original shear stress–shear rate curve (actual viscosity). The result is presented in Fig. 11 ( $H=313$  kA/m) together with the linear fit with the equation

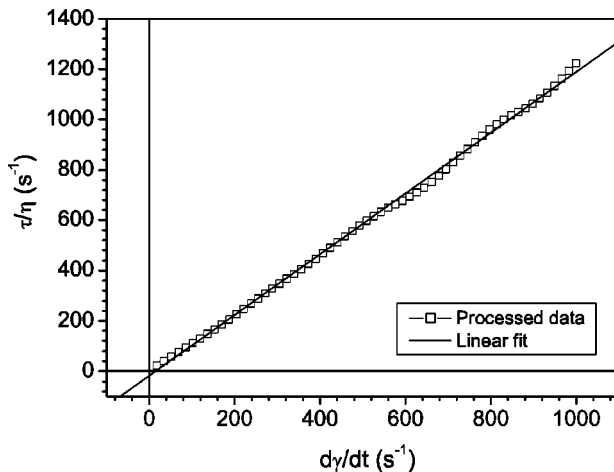


FIG. 11. Ratio of shear stress to actual viscosity, numerically obtained from the measured shear stress–shear rate curve, for 2.5% plates inverse magnetic fluid vs shear rate ( $H=313$  kA/m).

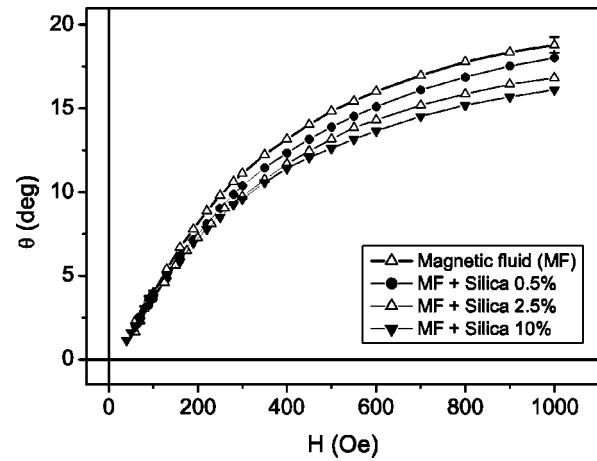


FIG. 12. Birefringence of silica inverse magnetic fluids vs applied magnetic field. A decaline-based ferrofluid with a volume fraction of magnetite of 2% was used in this case.

$\tau/\eta=(1/n)\dot{\gamma}$ , which led to  $n=0.81$ , close to the value obtained by fitting of  $\tau-\dot{\gamma}$  curve with Eq. (23) ( $n=0.86$ ).

Hexagonal plates IMF have not been prepared until now, but flow curves of similar silica inverse ferrofluids, in the presence of magnetic field only, were previously reported in Ref. [14]. However we measured a magnetoviscous effect even for the magnetic fluid matrix, while in Ref. [14], it was not measurable and we found a non-Newtonian behavior in zero field. Even though the magnetoviscous effect of the 10% silica IMF has the same order of magnitude as in our measurements, the derivative of Eq. (24) describes our data less accurate at higher shear rates than in Ref. [14], with a value of  $-0.92$  for the exponent of  $\dot{\gamma}$ .

For the case of 10% silica IMF, we could fit the data presented in Fig. 9 at very low shear rates only ( $0.015-0.035$  s $^{-1}$ ) with the Bingham model:  $\tau=\tau_0+\eta_B\dot{\gamma}$ , where  $\tau_0$  is the yield stress. A value of 0.59 Pa for the yield stress was found. In the other cases the low shear rate region was not accessible.

#### D. Magneto-optical properties of inverse magnetic fluids

First, measurements were done on silica and plates inverse ferrofluids. The ferrofluid matrices were based on cyclohexane and decaline. The ferrofluid based on decaline has a 2% volume fraction of magnetite (diluted in order to improve the transmission through the sample and to make possible dichroism measurements) while the ferrofluid based on cyclohexane, a volume fraction of 5.7%. Alumina particles were dispersed in a different magnetic fluid ( $\approx 4.5\%$  vol) prepared by D. Bica; it is the TR30 based sample described and studied in Ref. [20], and contains very small aggregates. In the last case, the magnetic particles were redispersed in decaline. The samples were prepared as for susceptibility measurements.

Only low volume fraction dispersions are analyzed. In this case, the magnetic field produced by the holes affects negligibly the magnetic fluid matrix and its magneto-optical properties.

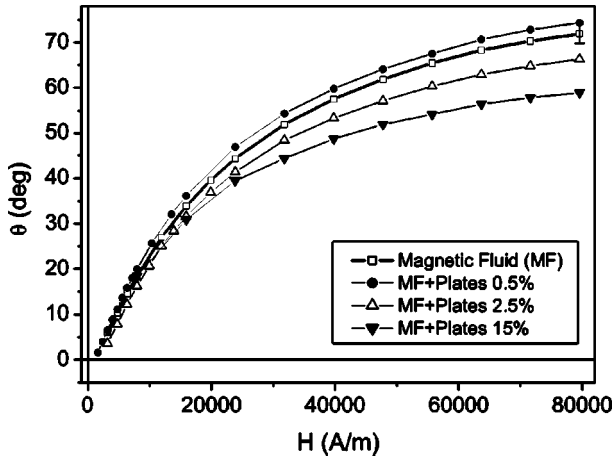


FIG. 13. Birefringence of plates inverse magnetic fluids vs applied magnetic field. A cyclohexane-based ferrofluid with a volume fraction of magnetite of 5.7% was used for these samples.

*Magnetobirefringence* measurements of silica inverse ferrofluids are presented in Fig. 12 and of gibbsite plates inverse ferrofluids in Fig. 13. The carrier liquids of MF were decaline (index of refraction  $n=1.4810$ ) and cyclohexane ( $n=1.4266$ ), respectively. Similar results were obtained for the case of silica particles in cyclohexane-based magnetic fluid. The increase in birefringence, because of silica chain formation and cluster formation/orientation of plates, respectively, was not observed.

We try to analyze the experimental facts below, first for silica dispersions. By dispersing silica spheres (in general nonmagnetic particles), we dilute the strongly birefringent ferrofluid. The volume fraction of magnetite particles in the inverse ferrofluids becomes  $\Phi'_0 = \Phi_0(1 - \Phi)$ .

The relative permittivity of silica to that of the ferrofluid matrix also influences the effect. This may come out if a similar approach as in Sec. III B is employed to calculate the effective permittivity of the inverse ferrofluid. Starting from the definition of effective permittivity [Eq. (10)], we obtained for very low silica volume fractions,

$$\varepsilon_{\text{eff}\parallel} = \varepsilon_{f\parallel} + \frac{\Phi(\varepsilon_s - \varepsilon_{f\parallel})\varepsilon_{f\parallel}}{\varepsilon_{f\parallel} + (\varepsilon_s - \varepsilon_{f\parallel})\langle N \rangle}, \quad (26)$$

$$\varepsilon_{\text{eff}\perp} = \varepsilon_{f\perp} + \frac{\Phi(\varepsilon_s - \varepsilon_{f\perp})\varepsilon_{f\perp}}{\varepsilon_{f\perp} + (\varepsilon_s - \varepsilon_{f\perp})\frac{1 - \langle N \rangle}{2}}. \quad (27)$$

Directions  $\parallel, \perp$  are again relative to the direction of the applied magnetic field,  $\varepsilon_s$  is the permittivity of silica, and  $\langle N \rangle$  is the mean depolarizing factor of chains (a mean value must be taken because of chain polydispersity). A change in notations occurred, to make equations clearer:  $\varepsilon_{f\parallel}$  is the quantity given by Eq. (7) and  $\varepsilon_{f\perp}$  by Eq. (6). The birefringence can be calculated by using Eq. (8). This model is correct within the *Rayleigh approximation only*, i.e.,  $D \ll \lambda_0$ . Our attempt to measure in infrared region failed because the transmission was not good enough in our setup (probably due to a too weak laser). At the wavelength we measured ( $\lambda_0$

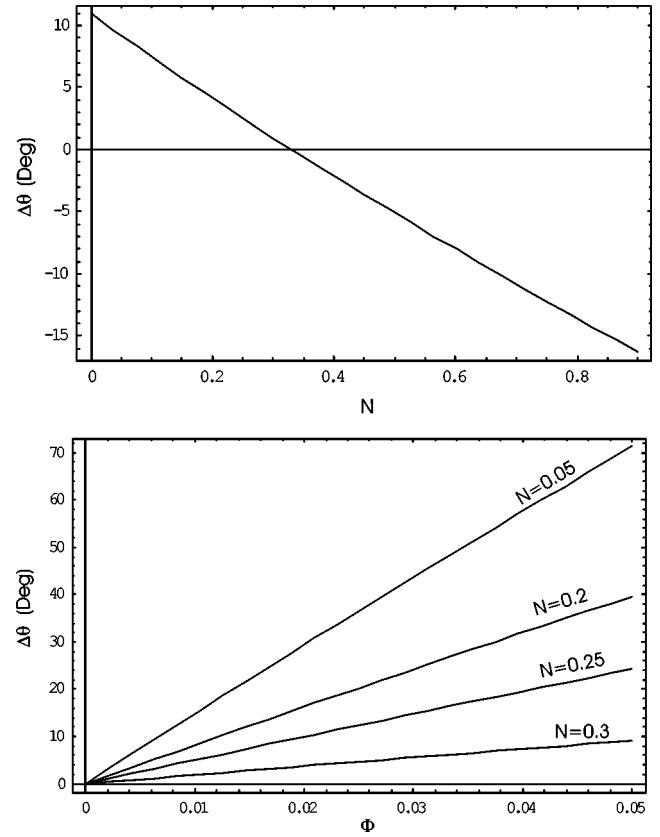


FIG. 14. Difference in birefringence of an inverse magnetic fluid and magnetic fluid matrix vs depolarization factor  $N$  ( $\Phi=0.5\%$ ) and volume fraction  $\Phi$  of nonmagnetic particles, calculated using Eqs. (8), (26), and (27). The value of the nonmagnetic particle permittivity was 3.115 (the permittivity for alumina) and the value of the ferrofluid permittivity was 2.119.

$=820$  nm), the above model does not work (we cannot define an effective dielectric tensor), so it could be that the increase in birefringence does not take place.

Within the frame of Rayleigh approximation, Eqs. (26) and (27) show that, depending on the values of  $\langle N \rangle$  and  $\Phi$ , the birefringence of the inverse ferrofluid can be smaller or larger than that of the ferrofluid matrix (Fig. 14); if aggregates oriented perpendicular to the magnetic field, the birefringence of the inverse ferrofluid would never be larger than that of the ferrofluid. However, even though long aggregates parallel to the magnetic field form, their effect upon birefringence may not be observed if the permittivity of silica is very close to that of the ferrofluid (Fig. 15).

For decaline-based samples (Fig. 12), the particularity was the lower concentration of magnetite in the ferrofluid matrix in comparison with the silica IMFs studied in Sec. III C, Fig. 9, which exhibited large silica chains, also confirmed by optical microscopy. A 1:1 dilution with decaline of the sample mentioned (originally 10% magnetite ferrofluid containing 10% dispersed silica), did not affect the optical microscopy image in the presence of the same magnetic field [the image was similar to that of Fig. 2(b)], but a 1:3 dilution with decaline of the same sample (the obtained sample is similar to that measured here), exhibited no visible magnetic

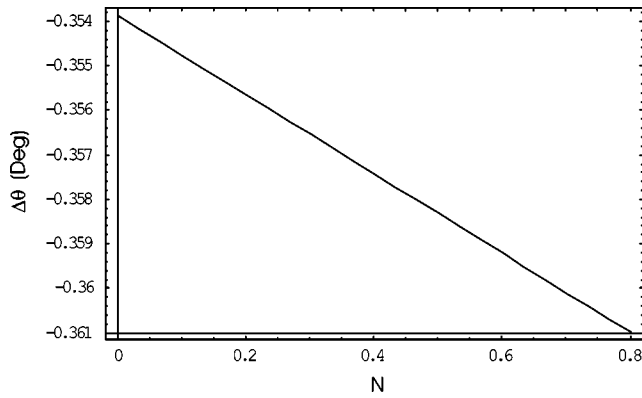


FIG. 15. Difference in birefringence of an inverse magnetic fluid and magnetic fluid matrix vs depolarization factor of nonmagnetic particles, calculated using Eqs. (8), (26), and (27). The value of the nonmagnetic particle permittivity was 2.1025 (the permittivity for silica) and the value of the ferrofluid permittivity was 2.119. The volume fraction of nonmagnetic particles was 0.5%. No increase in birefringence is predicted.

hole chains, which was unexpected because the dipole-dipole energy between two magnetic holes for this system at 0.1 T is of the order of 9 kT. For this estimation we used a generalization of Eq. (1) for higher fields. Thus, no additional anisotropy due to magnetic holes is present in this sample. It seems that the concentration of the magnetic fluid matrix affects significantly the structure formation of holes, a phase transition being possible. Further studies are necessary to explain what we observed here, this complex phenomenon being dependent on the magnetic field value, microstructural properties of the magnetic fluid, size of magnetic holes, and volume fractions of both types of dispersed particles. We can also conclude that for our systems and at higher fields, Eq. (1) does not describe correctly the moment of the holes in our systems.

In the case of cyclohexane-based samples, optical microscopy shows aggregation of holes (the concentration of magnetite in this ferrofluid matrix was higher). Before drawing the final conclusion, we mention that we observe that while the (negative) “dilution” contribution is always present, it is possible in this case that the (positive) effect due to chaining to be masked by the too small difference in permittivities. The permittivity of silica is  $\epsilon_s = 2.103$ , while the determined permittivity of the ferrofluid was 2.119, so that the difference could be small enough to mask the effect of aggregates (Fig. 15). Other explanations are also possible here. It is possible that the aggregates formed by the magnetic holes to have a smaller anisotropy than those of the displaced magnetic fluid (we recall that the aggregates in the magnetic fluid are quite large, being visible with an optical microscope). Thus we changed the magnetic fluid used until now with the “aggregate free” magnetic fluid, in which alumina particles were dispersed so that the optical contrast is higher. No increase in birefringence was observed, even though the sample is anisotropic, as it was shown by the optical microscopy. It seems now that, indeed, the effect is not present at wavelengths smaller than the length of the hole structures, even though their thickness is comparable to the wavelength.

Larger wavelengths must be tried.

In the case of platelets (smaller than silica spheres and very thin), the small increase observed for the 0.5% sample is of the order of experimental reproducibility and thus not interpretable. The permittivity of gibbsite particles is larger than that of silica (the average permittivity of gibbsite is  $\epsilon_g = 2.484$ ), but the structures are smaller (not observed by optical microscopy, observed in magnetorheological measurements but for a more concentrated ferrofluid matrix). Orientation of platelets seems not to play any role in these samples at these fields (dichroism also decreased). Consequently, the “dilution” of the MF matrix with gibbsite is still not overcompensated by the anisotropy of the nonmagnetic phase.

*Magnetodichroism* can be treated more rigorously. The small difference in the permittivities of nonmagnetic particles and ferrofluid may be regarded as an advantage and allows one to use the relatively simple Rayleigh-Gans-Debye (RGD) theory of scattering. Extremely small differences may, however, cause problems.

We have to add two contributions: (1) the anisotropic absorption due to magnetite particles  $\Delta n''_{abs}$ , and (2) the anisotropic scattering due to nonmagnetic particles:

$$\Delta n''_{sca} = \frac{\lambda_0}{4\pi} (\tau_{\parallel} - \tau_{\perp}), \quad (28)$$

where  $\tau_{\parallel, \perp}$  are the turbidity coefficients for parallel and perpendicular polarization of the incident light relative to the magnetic field direction. They are defined by the extinction law

$$I_t = I_0 \exp(-\tau l), \quad (29)$$

where  $I_0$  and  $I_t$  are the incident and transmitted light intensities through a sample of thickness  $l$ , respectively. Equation (29) is further on equivalent with  $I_t = I_0 \exp(-4\pi n'' l / \lambda_0)$ .

(1) We may think of relating  $\Delta n''_{abs}$  to the measured dichroism of the pure magnetic fluid matrix  $\Delta n''_f$ , defined as the difference  $n''_{\parallel} - n''_{\perp}$  of the imaginary components of the refractive indices for extraordinary and ordinary waves. In the case of magnetic fluids, the contribution of absorption to magnetodichroism is dominant [41] in comparison with that of scattering due to the small magnetic particles (which are Rayleigh scatterers). If large aggregates of magnetic particles form, scattering also contributes to the dichroism of the magnetic fluid as it was observed, for example, in Ref. [19]. That is why we preferred to replace the magnetic fluid matrix described in Sec. III A with the “aggregate free” magnetic fluid mentioned in the beginning of Sec. III D. It also contains magnetite particles covered with pure oleic acid, but only the presence of dimers and trimers was found significant [20].

Speaking only about absorption, the dichroism of the inverse magnetic fluids is apparently decreased because of the dilution of the magnetic fluid with holes (actually the decrease always occurs). The absorption due to holes themselves is completely negligible because we used practically transparent particles, like silica and alumina. If the holes are

not aggregated, we may write at first sight  $\Delta n''_{abs} = (1 - \Phi)\Delta n''_f$ , if the magnetic fluid is diluted enough, not aggregated, and particle interactions are negligible [it obeys then Eq. (9)]. But if the holes are aggregated into linear chains, the extraordinary wave is less absorbed than the ordinary wave.

(2) In this paper we focus, however, on the anisotropic scattering due to aggregated holes  $\Delta n''_{sca}$ , according to the following comments. Starting from the discussion in the above paragraph, the significant scattering contribution comes from the aggregated holes only. They also contribute to the magnetodichroism of the inverse magnetic fluid by means of the anisotropic absorption (at the inverse magnetic fluid scale), but that can be less important than the anisotropic scattering contribution. It was shown [41], for ferrofluids, that if the average volume of aggregates  $V_{agg}$  is larger than  $\lambda_0^3$ , the anisotropic absorption contribution becomes negligible. The Rayleigh scattering cross section was used in Ref. [41], but actually large aggregates are not Rayleigh scatterers anymore. In such a case the RGD model is better (if optical contrast is low enough), and it can be obtained if the Rayleigh scattering equation is multiplied by form and structure factors [see Eq. (30)]. But the term  $V_{agg}/\lambda_0^3$  remains (in the final equation for the transmission coefficients) and plays the same role. Neglecting the anisotropic absorption contribution still depends on the optical contrast and can be done at large enough values of contrast, which actually enhances the scattering. Generally speaking, however, both effects may be important and useful for applications.

Further on, we discuss only the contribution of the spherical nonmagnetic particles, which aggregate in the presence of a magnetic field. The turbidity is given by [42]

$$\tau = \frac{k_0^4}{(4\pi)^2} \rho V_p^2 \left| \frac{\varepsilon}{\varepsilon_{sol}} - 1 \right|^2 \times \int_0^\pi \int_0^{2\pi} P(\theta, \phi) S(\theta, \phi) f(\theta, \phi) \sin \theta d\theta d\phi, \quad (30)$$

where  $k_0$  is the incident wave vector,  $\rho$  is the particle number density of scatterers,  $V_p$  is the volume of one scatterer,  $\varepsilon$  is the permittivity of the scatterer,  $\varepsilon_{sol}$  is the permittivity of the solvent,  $P$  is the form factor,  $S$  is the structure factor, and  $f$  is the cosine of the angle between the polarization directions of the incident and scattered light. The magnetic hole chains, in the presence of a magnetic field, which are the scatterers in our case, can be modeled as circular cylinders parallel to the magnetic field direction, with diameter  $D$  and length  $L = n_c D$ , where  $n_c$  is the number of spheres in a cylinder. For dilute dispersions of cylinders  $S=1$ . The permittivity of magnetic holes  $\varepsilon_s$  is practically real but the permittivity of the ferrofluid is complex and anisotropic [according to Eqs. (6) and (7)]. However, the imaginary parts were found to be much smaller than the real parts. The function  $f$  depends on the polarization of the incident light and has the expression  $f_{\parallel}(\theta, \phi) = \cos^2 \phi + \sin^2 \phi \cos^2 \theta$  for parallel polarization and  $f_{\perp}(\theta, \phi) = \sin^2 \phi + \cos^2 \phi \cos^2 \theta$  for perpendicular polarization (Fig. 16). The form factor for cylinders is given by [37]

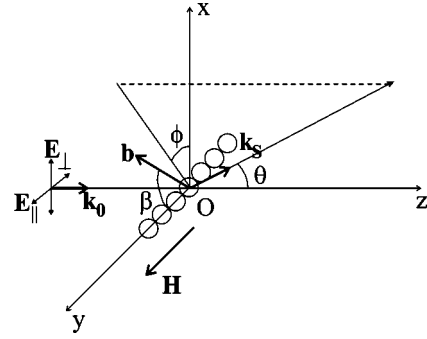


FIG. 16. Experimental configuration for the case of light scattering by aggregated magnetic holes in a magnetic field. The unit vector  $\mathbf{b}$  denotes the direction of  $\mathbf{k}_s - \mathbf{k}_0$ . Notations  $E_{\parallel}$  and  $E_{\perp}$  corresponds to the waves polarized parallel and perpendicular to the magnetic field, respectively (extraordinary and ordinary waves).

$$P_c(\theta, \phi) = \frac{\pi}{2v \cos \beta} \left[ J_{1/2}(v \cos \beta) \frac{2J_1(u \sin \beta)}{u \sin \beta} \right]^2, \quad (31)$$

where  $J_1$  and  $J_{1/2}$  are Bessel's functions,  $u = 2k_0 D \sin(\theta/2)$ ,  $v = k_0 L \sin(\theta/2)$ , and  $\beta$  is the angle between the cylinder axis and the direction  $\mathbf{k}_s - \mathbf{k}_0$ , where  $\mathbf{k}_s$  is the scattered wave vector. For cylinders perpendicular to  $\mathbf{k}_0$ , one obtains (according to the notations in Fig. 16)

$$\cos \beta = \cos \frac{\theta}{2} \sin \phi. \quad (32)$$

Finally, we obtained for the turbidity coefficients for ordinary and extraordinary waves,

$$\tau_{\parallel, \perp} = \frac{k_0^4}{(4\pi)^2} n_c \Phi \frac{\pi D^3}{6} \left[ \left( \frac{\varepsilon_s}{\varepsilon'_{f\parallel, \perp}} - 1 \right)^2 + \frac{\varepsilon_s^2 \varepsilon''_{f\parallel, \perp}}{\varepsilon'^2_{f\parallel, \perp}} \right] \times \int_0^\pi \int_0^{2\pi} P_c(\theta, \phi, n_c) f_{\parallel, \perp}(\theta, \phi) \sin \theta d\theta d\phi. \quad (33)$$

If the form factor depends on  $\theta$  only (as for spheres) then  $\tau_{\parallel} = \tau_{\perp}$ . The contribution due to shape anisotropy of particles to dichroism is thus determined by the dependence on  $\phi$  only, because the form factor does not depend on polarization. The dependence on magnetic field is related to the average length of the silica chains. In zero field there are no aggregated spheres, thus no dichroism due to magnetic holes, while in the presence of the magnetic field the chain length increases with the field. Of course there are clusters of silica in zero field but they do not contribute either to the dichroism because they are randomly oriented. An example of the calculated contribution to dichroism of silica and alumina chains relative to the dichroism of the magnetic fluid matrix at the highest magnetic field attained in our experiments, for several average numbers of particles per chain, by using Eqs.

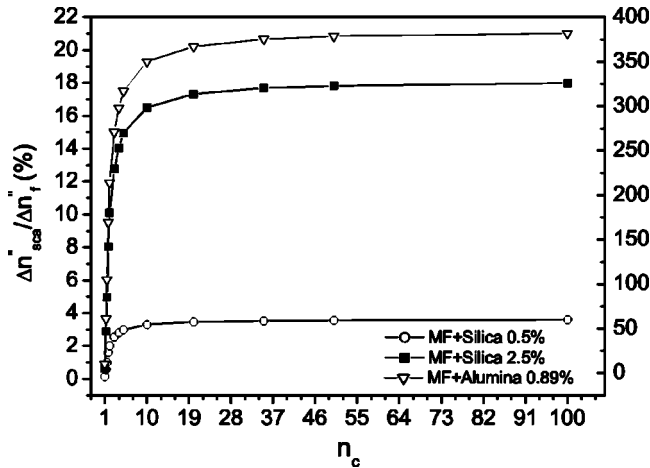


FIG. 17. Theoretical relative increase in dichroism due to the anisotropic scattering generated by silica and alumina chains which may form in a magnetic fluid (MF) vs the average number of particles per chain. The right scale applies for alumina inverse ferrofluid only.

(28) and (33), led to the results presented in Fig. 17. The measured dichroism of 2% decaline-based pure magnetic fluid was used here.

Alternatively, the form factor for spherical holes can be used in Eq. (30), but then the structure factor must be calculated as a function of magnetic field.

The model presented here is quantitatively valid as long as RGD model is valid. Its applicability is limited by the chain size (for a certain type of particles and solvent): in our case, the silica chains may contain up to 100 particles, while in the case of alumina, which has a higher permittivity, only a few particle chains can be described with our model.

Alumina particles with a volume fraction of  $\Phi = 0.89\%$  were dispersed in the “aggregate free” magnetic fluid (with a volume fraction of magnetite of approximately 4.5%). The results are presented in Fig. 18. We observe in this case a significant increase in magnetodichroism in comparison with

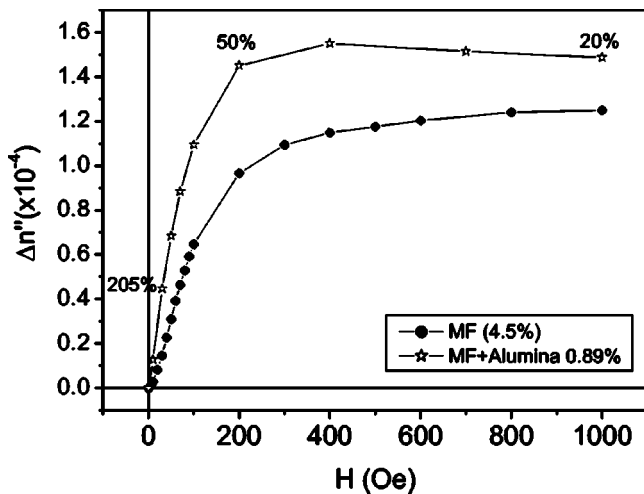


FIG. 18. Dichroism of alumina inverse ferrofluid vs applied magnetic field.

that of the magnetic fluid matrix, which is within the predicted limits of our model. At higher fields the dichroism decreases. This is a result of chain-chain interactions, which lead to thick chain formation, with a smaller aspect ratio; it decreases the dichroism of the sample in time. Chain association was confirmed by the images taken with an optical microscope.

#### IV. CONCLUSIONS

We have prepared new inverse magnetic fluids containing gibbsite plates and alumina spheres by grafting the particles with polyisobutene and dispersing them in apolar magnetic fluids. Silica inverse magnetic fluids have also been prepared. All these systems are remarkably homogeneous and stable, as it was shown by optical microscopy and atomic force microscopy investigations. No measurable changes occurred in the the magnetic phase of these systems after dispersing the nonmagnetic particles, as it was shown by alternating gradient magnetometry. In the presence of a magnetic field, the aggregation of spherical magnetic holes was optically observed. Optical microscopy also evidenced the presence of magnetic particle aggregates in the pure magnetic fluid.

Particles were characterized using various techniques: atomic force microscopy, transmission electron microscopy, alternating gradient magnetometry, and static and dynamic light scattering. The methods, results, and the differences between the determined values were discussed.

The initial susceptibility of inverse ferrofluids was calculated in the case of noninteracting and interacting nonmagnetic particles, by calculating the effective susceptibility of a mixture of magnetic holes in a continuous magnetizable medium. The agreement with the experimental data was very good, so that the “dilution” equation for magnetization, previously observed, is not valid at small fields.

The magnetorheological cell for Physica MCR 300 rheometer, done for magneto-rheological fluids, could also be used for measuring the flow curves of moderately concentrated inverse magnetic fluids in the whole range of shear rates. The other samples were possible to measure at higher shear rates only.

The flow curves were measured in the absence and in the presence of a magnetic field. In spite of the aggregates present in the magnetic fluid, it remained Newtonian at all fields (in the shear rate range in which we had enough sensitivity to measure), exhibiting a 40% effect at the highest field. The inverse magnetic fluids were non-Newtonian at all fields and a significant magnetorheological effect was noticed in the case of the moderately concentrated (10%) silica inverse ferrofluid. An improved form of power law fitted well most of the  $\tau - \dot{\gamma}$  curves. The non-Newtonian behavior of silica inverse ferrofluids in zero field was explained mainly by the presence of preformed clusters (due to the van der Waals interaction) of nonmagnetic particles, and, in the case of the more concentrated sample (10%) by particle interactions too. Their magnetorheological effect was due to the chaining of silica particles (due to the dipole-dipole interaction). In the case of platelets inverse magnetic fluid, the

effect was explained by the aggregation of the preformed clusters of platelets. The disruption of aggregates, caused by the shear flow, explains the shear thinning. In the case of platelets, only at high shear rates, shear flow orientation of particles may occur, but this effect was considered not important. No rigorous conclusion about magnetic field orientation of plates could be inferred, but, if it occurred in our experiments, its influence on the magnetoviscous effect of plates inverse ferrofluid was supposed to be small. We demonstrated the validity of the power law in the case of flow curves of plates inverse ferrofluid, but that takes place in a rather small range of shear rates.

The static magnetobirefringence of silica, plates, and alumina inverse magnetic fluids was measured, modeled within the Rayleigh approximation, and discussed. The birefringence of silica/alumina inverse ferrofluids decreases in comparison to the birefringence of the magnetic fluid. An increase might be observed at large wavelengths only. In the case of gibbsite plates inverse ferrofluids, the insignificant orientation of platelets in the external magnetic field and the small aggregation in the measured samples were not able to overcompensate the “dilution” of the ferrofluid matrix.

The unexpected disappearance (from the optical microscope images) of magnetic hole chaining showed that the concentration, together with the microstructural properties of the magnetic fluid, play an important role in magnetic hole aggregation (a fact not studied yet). Further studies are necessary to clarify this phenomenon.

The contribution of nonmagnetic particle chains to the static magnetodichroism was theoretically calculated and

discussed, in the frame of the Rayleigh-Gans-Debye theory of scattering. The effect was observed when alumina particles were dispersed in an “aggregate free” magnetic fluid. The fact that the effect decreased with the field (relative to that of the magnetic fluid) was explained by the presence of chain-chain interactions.

In conclusion, at a wavelength of 820 nm, our samples exhibit a smaller birefringence but a higher dichroism after nonmagnetic particles were dispersed in the magnetic fluid.

#### ACKNOWLEDGMENTS

Magnetorheological measurements were done at the National Center for Complex Fluid Engineering (“Politehnica” University of Timisoara, Romania). Dr. L. Vekas, Dr. D. Resiga, and O. Balau are thanked for instructions in operating the magnetorheometer; Dr. F. Stoian is acknowledged for performing some VSM measurements, and Dr. D. Bica for providing us with the magnetic fluids. We thank to Dr. M. van Bruggen (Philips Research, The Netherlands) for providing the alumina powder and for useful suggestions. Professor G. Noyel and Professor J. J. Rousseau (DIOM Laboratory, University Jean Monnet, Saint-Etienne, France) are acknowledged for facilitating the cooperation between our labs in the field of magneto-optics. Dr. A. Petukhov (Van ‘t Hoff Laboratory) is acknowledged for helpful discussions. This work was financially supported by the Colloid Physics Stimulation Program initiated by Professor H. Lekkerkerker and Dr. G. van Ginkel and awarded by the University of Utrecht.

- 
- [1] E. Blums, A. Cebers, and M. M. Maiorov, *Magnetic Fluids* (Walter de Gruyter, Berlin, 1997), pp. 1, 343.
  - [2] R. E. Rosensweig, *Ferrohydrodynamics* (Cambridge University Press, Cambridge, 1985).
  - [3] K. Raj, in *Magnetic Fluids and Applications Handbook*, edited by B. Berkovski and V. Bashtovoi (Begell House, New York, 1996), p. 657.
  - [4] O. Volkova, G. Bossis, M. Guyot, V. Bashtovoi, and A. Reks, *J. Rheol.* **44**, 91 (2000).
  - [5] A.F. Pshenichnikov and P.A. Sosnin, *J. Exp. Theor. Phys.* **95**, 275 (2002).
  - [6] A.T. Skjeltorp, *Phys. Rev. Lett.* **51**, 2306 (1983).
  - [7] A.T. Skjeltorp and G. Helgesen, *Physica A* **176**, 37 (1991).
  - [8] A.T. Skjeltorp, *J. Appl. Phys.* **55**, 2587 (1984).
  - [9] A.T. Skjeltorp, *J. Appl. Phys.* **57**, 3285 (1985).
  - [10] P.C. Fannin, S.W. Charles, and A.T. Skjeltorp, *J. Magn. Magn. Mater.* **201**, 113 (1999).
  - [11] M.H. Lu and C. Rosenblatt, *Appl. Phys. Lett.* **56**, 590 (1990).
  - [12] B.E. Kashevskii, V.I. Kordonskii, and I.V. Prokhorov, *Magn. Hidrodin.* **3**, 121 (1988).
  - [13] J. Popplewell and R.E. Rosensweig, *J. Phys. D* **29**, 2297 (1996).
  - [14] B.J. de Gans, Ph.D. thesis, University of Twente, 2000.
  - [15] B.J. de Gans, C. Blom, A.P. Philipse, and J. Mellema, *Phys. Rev. E* **60**, 4518 (1999).
  - [16] G. van Ewijk, Ph.D. thesis, Utrecht University, 2000.
  - [17] J.D. Jackson, *Classical Electrodynamics* (Wiley, New York, 1975), p. 151.
  - [18] B.J. de Gans, C. Blom, J. Mellema, and A.P. Philipse, *J. Magn. Magn. Mater.* **201**, 11 (1999).
  - [19] V. Socoliuc *et al.*, *J. Magn. Magn. Mater.* **191**, 241 (1999).
  - [20] M. Raşa, D. Bica, A. Philipse, and L. Vekas, *Eur. Phys. J. E* **7**, 209 (2002).
  - [21] A.O. Ivanov, *Magn. Hidrodin.* **4**, 39 (1992).
  - [22] A.O. Ivanov and O.B. Kuznetsova, *Colloid J.* **63**, 60 (2001).
  - [23] M.I. Shliomis, *J. Exp. Theor. Phys.* **61**, 2411 (1972).
  - [24] L. Vekas, M. Raşa, and D. Bica, *J. Colloid Interface Sci.* **231**, 247 (2000).
  - [25] V. Socoliuc, *J. Magn. Magn. Mater.* **207**, 146 (1999).
  - [26] M. Raşa, *J. Magn. Magn. Mater.* **201**, 170 (1999).
  - [27] M. Raşa, *Eur. Phys. J. E* **2**, 265 (2000).
  - [28] J.J.M. Janssen and J.A.A. Perenboom, *J. Magn. Magn. Mater.* **81**, 14 (1989).
  - [29] D. Bica, *Rom. Rep. Phys.* **47**, 265 (1995).
  - [30] A.M. Wierenga and A.P. Philipse, *J. Colloid Interface Sci.* **180**, 360 (1996).
  - [31] F.M. van der Kooij and H.N.W. Lekkerkerker, *J. Phys. Chem. B* **102**, 7829 (1998).
  - [32] M. Raşa, B.W.M. Kuipers, and A.P. Philipse, *J. Colloid Interface Sci.* **250**, 303 (2002).

- [33] F. Donatini, D. Jamon, J. Monin, and S. Neveu, *IEEE Trans. Magn.* **35**, 4311 (1999).
- [34] D. Jamon, Ph.D. thesis, Université Jean Monnet, 2000.
- [35] J.K.G. Dhont, *An Introduction to Dynamics of Colloids* (Elsevier, Amsterdam, 1996), p. 129.
- [36] J.K.G. Dhont, *An Introduction to Dynamics of Colloids* (Ref. [35]), p. 164.
- [37] M. Kerker, *The Scattering of Light* (Academic Press, New York, 1969), p. 485.
- [38] L.D. Landau, E.M. Lifshitz, and L.P. Pitaevskii, *Electrodynamics of Continuous Media* (Pergamon Press, Oxford, 1984), p. 42.
- [39] L.D. Landau, E.M. Lifshitz, and L.P. Pitaevskii, *Electrodynamics of Continuous Media* (Ref. [38]), p. 41.
- [40] K. Wollny, J. Lauger, and S. Huck, *Appl. Rheol.* **12**, 25 (2002).
- [41] S. Taketomi, S. Ogawa, H. Miyajima, and S. Chikazumi, *IEEE Transl. J. Magn. Jpn.* **4**, 384 (1989).
- [42] J.K.G. Dhont, *An Introduction to Dynamics of Colloids* (Ref. [35]), p. 527.